Nodeless superconductivity and the peak effect in the quasiskutterudites $Lu_3Os_4Ge_{13}$ and $Y_3Ru_4Ge_{13}$

Z. F. Weng,[1] M. Smidman,[1,*] G. M. Pang,[1] O. Prakash,[2] Y. Chen,[1] Y. J. Zhang,[1] S. Ramakrishnan,[2] and H. Q. Yuan[1,3,†]

[1]*Center for Correlated Matter and Department of Physics, Zhejiang University, Hangzhou 310058, China*

[2]*Department of Condensed Matter Physics and Materials Science, Tata Institute of Fundamental Research, Mumbai 400005, India*

[3]*Collaborative Innovation Center of Advanced Microstructures, Nanjing 210093, China*

(Received 18 January 2017; revised manuscript received 24 March 2017; published 1 May 2017)

We report an investigation of the superconducting states of $Lu_3Os_4Ge_{13}$ and $Y_3Ru_4Ge_{13}$ single crystals by measurements of the electrical resistivity, ac susceptibility, and London penetration depth. The analysis of the penetration depth and the derived superfluid density indicates the presence of nodeless superconductivity and suggests that there are multiple superconducting gaps in both materials. Furthermore, ac susceptibility measurements of both compounds display the peak effect in the low-temperature region of the H-T phase diagram. This anomalous increase of the critical current with field gives an indication of a change of the arrangement of flux lines in the mixed state, as found in some of the isostructural stannide materials.

DOI: 10.1103/PhysRevB.95.184501

I. INTRODUCTION

Since the discovery of the ternary superconducting stannides $R_3T_4M_{13}$ [1,2], numerous compounds with this stoichiometry have been synthesized, where R is an alkaline earth or rare earth metal, T is a transition metal, and M is one of In, Si, Ge, Sn, or Pb. At room temperature, most of these materials crystallize in the primitive cubic $Yb_3Rh_4Sn_{13}$ type structure with the space group $Pm\bar{3}n$ [2]. In this caged structure, R and T atoms each occupy one crystallographic site, while there are two sites for M, where the M atom on one site is surrounded by a polyhedral cage formed from the M atoms on the other site. There are a few examples of compositions with different structures, such as tetragonal $Yb_3Pt_4Ge_{13}$ [3], monoclinic $Y_3Pt_4Ge_{13}$ [4], and $U_3Ir_4Ge_{13}$, which has a noncentrosymmetric rhombohedral structure [5]. The $R_3T_4M_{13}$ compounds have attracted considerable interest since they display a wide range of physical properties, such as superconductivity [1,4,6–14], magnetism [5,15–18], mixed valence behavior [14,19–21], structural phase transitions, and quantum criticality [22,23].

Particular attention has been paid to the stannides $R_3T_4Sn_{13}$. $Sr_3Rh_4Sn_{13}$ and $Sr_3Ir_4Sn_{13}$ exhibit both a second-order structural phase transition and superconductivity, where the structural phase transition can be suppressed to lower temperatures by applying pressure or doping [22,23]. Non-Fermi-liquid behavior is observed when the structural phase transition temperature is tuned to zero, implying the existence of a structural quantum critical point. Evidence for strongly coupled nodeless superconductivity has been found in the stannides $R_3T_4Sn_{13}$ (R = La, Sr, Ca and T = Rh, Ir) from various measurements [6,7,24–26], where a strong enhancement of the coupling is found in the vicinity of the structural quantum critical point in $(Ca_xSr_{1-x})_3Rh_4Sn_{13}$ from the specific heat [27] and in $Ca_3Ir_4Sn_{13}$ from muon spin rotation (μSR) [28].

In comparison to the stannides, germanides with M = Ge which show a lack of a structural transition have received less attention. In many cases weak semiconducting behavior in the resistivity is observed and those materials which are superconductors have fairly low values of T_c [9]. The recent synthesis of high-quality single crystals of the germanide superconductors $Lu_3Os_4Ge_{13}$ [10] and $Y_3Ru_4Ge_{13}$ [11] offers new opportunities to investigate the superconducting properties of the $R_3T_4Ge_{13}$ series. Multiband superconductivity was suggested in $Lu_3Os_4Ge_{13}$ on the basis of specific heat measurements, which is consistent with the calculated complex Fermi surface where the density of states predominantly consists of contributions from Os and Ge [10]. Meanwhile, although $Y_3Ru_4Ge_{13}$ is metallic, band structure calculations suggest a broad minimum in the density of states in the vicinity of the Fermi level, which is mainly from Ge with little contribution from Ru d orbitals [29]. However, further characterization of the superconducting order parameter of both compounds is necessary. Here, we present measurements of the resistivity (ρ), ac susceptibility (χ), and change of the penetration depth [$\Delta\lambda(T)$] of $Lu_3Os_4Ge_{13}$ and $Y_3Ru_4Ge_{13}$ single crystals down to 0.4 K. The penetration depth of both materials flattens at low temperatures, indicating fully gapped superconductivity, and the calculated superfluid density $\rho_s(T)$ is well described by a two-gap s-wave model, indicating that $Lu_3Os_4Ge_{13}$ and $Y_3Ru_4Ge_{13}$ are nodeless, multiband superconductors. Furthermore, field-dependent ac susceptibility measurements at low temperatures show the presence of the peak effect in both compounds, which may indicate a change in the arrangement of vortices in the mixed state, as seen in some of the isostructural stannide materials.

II. EXPERIMENTAL DETAILS

$Lu_3Os_4Ge_{13}$ and $Y_3Ru_4Ge_{13}$ single crystals were grown using the Czochralski method in a tetra-arc furnace under an argon atmosphere, as described previously [10,11]. The electrical resistivity was measured in a ^{3}He cryostat utilizing a four-probe method. The ac susceptibility was measured in the same ^{3}He cryostat using an ac susceptometer. Note that the excitation current used was 100 μA, which corresponds to a magnetic field of around 0.4 Oe. Precise measurements of the penetration depth change $\Delta\lambda(T)$ were performed using a tunnel-diode oscillator (TDO) based, self-inductive technique at an operating frequency of 7 MHz down to 0.4 K in a ^{3}He

*msmidman@zju.edu.cn

†hqyuan@zju.edu.cn

cryostat, with which a noise level as low as 0.1 Hz can be obtained. The London penetration depth change is proportional to the change of the resonant frequency $\Delta f(T)$, i.e., $\Delta\lambda(T) = \lambda(T) - \lambda(0) = G\Delta f(T)$, where $\lambda(0)$ is the penetration depth at zero temperature and the G is calculated using the sample and coil geometries [30]. The coil of the oscillator generates a very small ac magnetic field ($H_{ac} \approx 20$ mOe), which is much less than the lower critical fields of $Lu_3Os_4Ge_{13}$ and $Y_3Ru_4Ge_{13}$ [10,11], ensuring that all the measurements were performed in the Meissner state.

III. RESULTS AND DISCUSSION

In order to characterize the samples, the temperature dependence of the electrical resistivity $\rho(T)$ and ac magnetic susceptibility $\chi(T)$ for $Lu_3Os_4Ge_{13}$ and $Y_3Ru_4Ge_{13}$ were measured, as shown in Fig. 1. Superconducting transitions are observed in the measurements for both compounds, with $T_c = 3.2$ and 3.05 K from the midpoints of the transitions in the resistivity, and ac susceptibility of $Lu_3Os_4Ge_{13}$, respectively, while the respective values for $Y_3Ru_4Ge_{13}$ are $T_c = 2.8$ and 2.3 K. Since the susceptibility is a bulk probe, the values of T_c from the ac susceptibility are used in the later analysis of the superfluid density.

A. Penetration depth and superfluid density

In Fig. 2 the temperature dependence of $\Delta\lambda(T)$ is shown for (a) $Lu_3Os_4Ge_{13}$ and (b) $Y_3Ru_4Ge_{13}$, which are converted

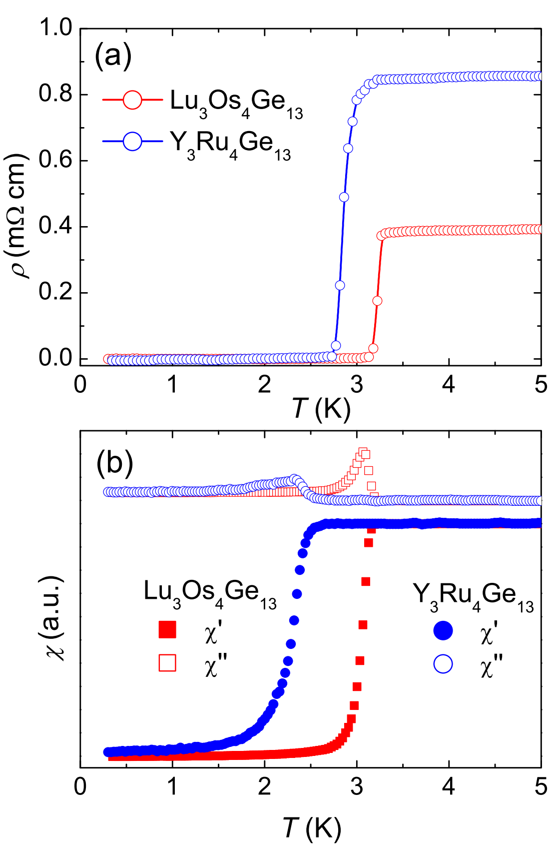

FIG. 1. Temperature dependence of (a) electrical resistivity and (b) ac susceptibility of $Lu_3Os_4Ge_{13}$ and $Y_3Ru_4Ge_{13}$.

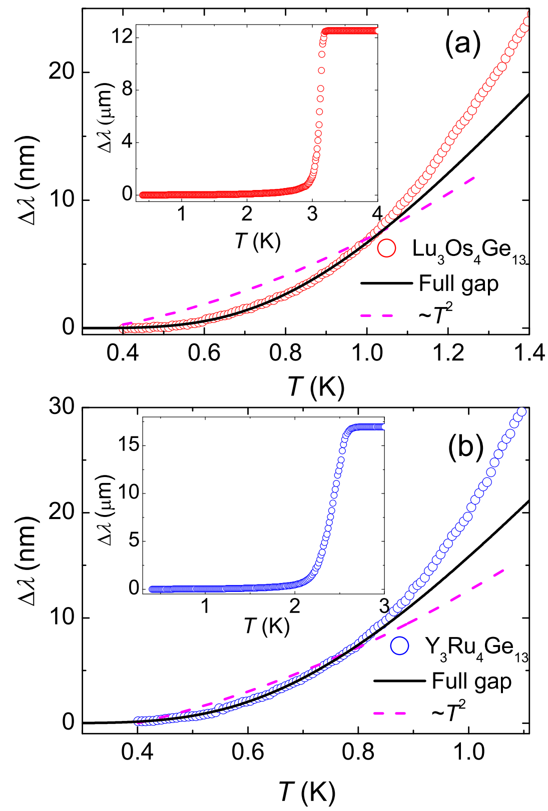

FIG. 2. Temperature dependence of the change of the London penetration depth $\Delta\lambda(T)$ at low temperatures of (a) $Lu_3Os_4Ge_{13}$ and (b) $Y_3Ru_4Ge_{13}$. The solid and dashed lines show fits of $\Delta\lambda(T)$ to a fully gapped model and a T^2 dependence, respectively. The insets show $\Delta\lambda(T)$ from the base temperature to above T_c.

from the frequency shift $\Delta f(T)$ with respective calibration constants of $G = 6.1$ Å/Hz and $G = 9.0$ Å/Hz. The insets display $\Delta\lambda(T)$ from above T_c down to the base temperature. In $Lu_3Os_4Ge_{13}$ a sharp superconducting transition with $T_c \simeq 3.05$ K is observed, which is the same value as obtained from the ac magnetic susceptibility, while $Y_3Ru_4Ge_{13}$ has a superconducting transition with a midpoint $T_c \simeq 2.4$ K, slightly higher than the ac susceptibility.

In the main panels of Figs. 2(a) and 2(b), the solid and dashed lines show the fits to a nodeless s-wave model and a model with point nodes ($\sim T^2$), respectively. It is clear that the point node model cannot describe the data, nor is there a linear temperature dependence as expected in the case of line nodes in the gap. Instead, the data flatten at low temperatures, which is not expected for nodal superconductivity, but indicates a fully open superconducting gap. For isotropic s-wave superconductors at $T \ll T_c$, $\Delta\lambda(T) \propto \sqrt{\frac{\pi\Delta(0)}{2k_BT}}e^{-\frac{\Delta(0)}{k_BT}}$, where $\Delta(0)$ is the gap magnitude at zero temperature. As shown in Fig. 2(a), the experimental data of $Lu_3Os_4Ge_{13}$ are well fitted in the low-temperature limit with an energy gap of $\Delta(0) = 1.35k_BT_c$. Fitting the data of $Y_3Ru_4Ge_{13}$ gives a gap value of $\Delta(0) = 1.5k_BT_c$, as shown in Fig. 2 (b). These values are smaller than the BCS value of $1.76k_BT_c$ expected for an isotropic, weakly coupled BCS superconductor, consistent with either gap anisotropy or multiband superconductivity.

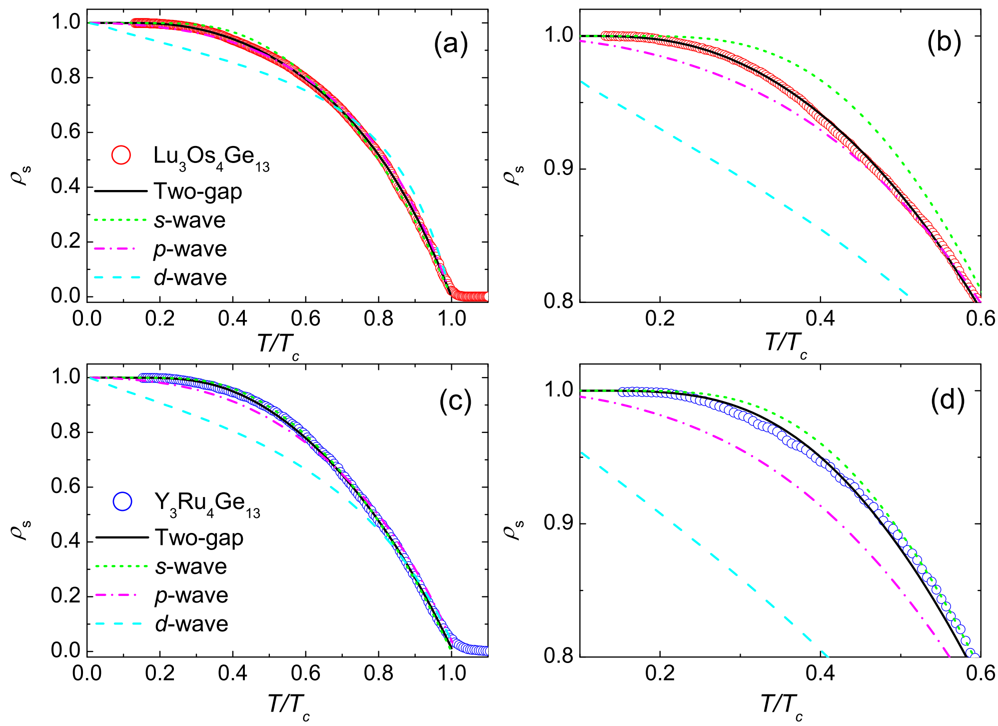

FIG. 3. Normalized superfluid density $\rho_s(T)$ along with fits to various models for (a) $Lu_3Os_4Ge_{13}$, where (b) displays an enlargement of the low-temperature region, and (c) $Y_3Ru_4Ge_{13}$, with (d) showing the low-temperature behavior.

To obtain more information about the gap structure of $Lu_3Os_4Ge_{13}$ and $Y_3Ru_4Ge_{13}$, the normalized superfluid density $\rho_s(T)$ was calculated from the London penetration depth using $\rho_s(T) = [\lambda(0)/\lambda(T)]^2$, where $\lambda(0) = 4736$ Å [10] and

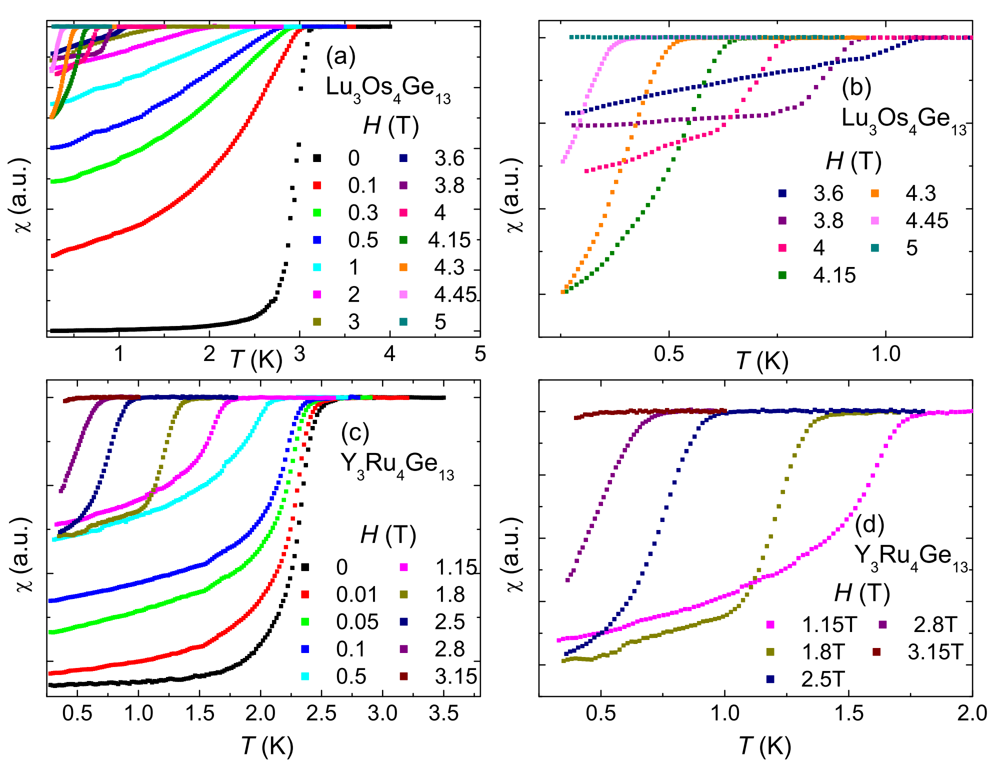

FIG. 4. (a) Temperature dependence of the ac susceptibility of $Lu_3Os_4Ge_{13}$ in various applied magnetic fields, where (b) shows an enlargement of the data for high applied fields. (c) Temperature dependence of the ac susceptibility of $Y_3Ru_4Ge_{13}$ in various applied magnetic fields, where (d) shows the high-field data.

4951 Å [11] are calculated from the critical fields of $Lu_3Os_4Ge_{13}$ and $Y_3Ru_4Ge_{13}$, respectively. The respective $\rho_s(T)$ of $Lu_3Os_4Ge_{13}$ and $Y_3Ru_4Ge_{13}$ are shown in Figs. 3(a) and 3(c). The normalized superfluid density is calculated using

$$\rho_s(T) = 1 + 2\left\langle \int_{\Delta_k}^{\infty} \frac{E dE}{\sqrt{E^2 - \Delta_k^2}} \frac{\partial f}{\partial E} \right\rangle_{\mathrm{FS}}, \quad (1)$$

where f is the Fermi function and $\langle \cdots \rangle_{\mathrm{FS}}$ denotes the average over the Fermi surface. The superconducting gap $\Delta_k(T,\theta,\varphi) = g_k(\theta,\varphi)\Delta(T)$ has an angular dependence $g_k(\theta,\varphi)$ and a temperature dependence given by [31]

$$\Delta(T) = \Delta(0)\tanh\{1.82[1.018(T_c/T - 1)]^{0.51}\}. \quad (2)$$

The flat behavior of the data at low temperatures for both materials clearly deviates from the behavior of nodal gap functions, i.e., a d-wave model (line nodes) $g_k(\theta,\varphi) = |\cos(2\varphi)|$ and a p-wave model (point nodes) $g_k(\theta,\varphi) = |\sin(\theta)|$. The data were also fitted using a single-band s-wave model, where the fitted energy gaps are $\Delta(0) = 2.13 k_B T_c$ and $\Delta(0) = 2.05 k_B T_c$ for $Lu_3Os_4Ge_{13}$ and $Y_3Ru_4Ge_{13}$, respectively, both larger than the isotropic BCS value of $1.76 k_B T_c$. It can be seen in Figs. 3(a) and 3(c) that this can describe the data at higher temperatures. However, as shown in the low-temperature enlargements in Figs. 3(b) and 3(d), at low temperatures the data drop more rapidly than expected for the single-band models. In particular, for $Lu_3Os_4Ge_{13}$ there is a significant deviation below $T/T_c \approx 0.6$, while the difference in the case of $Y_3Ru_4Ge_{13}$ is smaller, below $T/T_c \approx 0.5$. Such a low-temperature deviation from the fitted single-gap model would be expected, since considerably smaller gap values are obtained from fitting the low-temperature $\Delta\lambda(T)$. These results suggest the presence of multiple energy scales and multiband superconductivity, which is also consistent with the complex Fermi surface revealed by band structure calculations [10]. Therefore, the data were fitted using a two-gap model where the superfluid density is given by $\rho_s(T) = x\rho_1(T) + (1-x)\rho_2(T)$, where $\rho_i(T)$ is the superfluid density corresponding to a gap Δ_i and x is the weight of the contribution from Δ_1.

The data for both materials are well described by such a two-gap model, with fitted parameters of $\Delta_1(0) = 1.25 k_B T_c$, $\Delta_2(0) = 2.5 k_B T_c$, and $x = 0.22$ for $Lu_3Os_4Ge_{13}$, and $\Delta_1(0) = 1.4 k_B T_c$, $\Delta_2(0) = 2.15 k_B T_c$, and $x = 0.15$ for $Y_3Ru_4Ge_{13}$. In both cases the values of the smaller gap are close to those obtained from the low-temperature fit of the penetration depth shown in Fig. 2, as often found for two-band superconductors [32]. Therefore, the penetration depth measurements and the derived superfluid density $\rho_s(T)$ are all consistent with multiband superconductivity in $Lu_3Os_4Ge_{13}$ and $Y_3Ru_4Ge_{13}$, as also suggested from specific heat measurements [10,11]. It should be noted that the superfluid density of both compounds can also be fitted with an anisotropic s-wave model, and it is often difficult to distinguish between this scenario and two-gap superconductivity from thermodynamic measurements [32]. However, the three-dimensional cubic crystal structure and the presence of multiple bands crossing the Fermi level favor the two-gap scenario.

B. H-T phase diagram and the peak effect

In order to determine the field-temperature phase diagram and probe the properties in the mixed state of $Lu_3Os_4Ge_{13}$ and $Y_3Ru_4Ge_{13}$, isofield and isothermal ac susceptibility measurements were performed. Figure 4(a) displays the temperature dependence of the ac susceptibility of $Lu_3Os_4Ge_{13}$ in various applied magnetic fields, where the sample was cooled in zero field before data were collected upon warming to above T_c. In zero field, a sharp superconducting transition is observed, but upon increasing the field in the mixed state, the transition becomes broader and the shielding fraction is reduced. However, as shown in Fig. 4(b), when a field of 3.8 T is applied, the ac susceptibility is reduced at the lowest temperatures compared to 3.6 T, indicating an increase of the superconducting shielding fraction, although T_c continues to decrease. The shielding fraction continues to increase with increasing field until 4.15 T, above which the shielding is again reduced, and at 5 T no superconducting transition is observed in the ac susceptibility. Similar behavior is also found in $Y_3Ru_4Ge_{13}$ [Figs. 4(c) and 4(d)], where the shielding fraction again begins to increase above 1.15 T, before again decreasing between 1.8 and 2.5 T.

The field dependence of the ac susceptibility is also displayed for $Lu_3Os_4Ge_{13}$ in Fig. 5(a) and $Y_3Ru_4Ge_{13}$ in Fig. 5(b). The sample was first cooled to a given temperature and the data

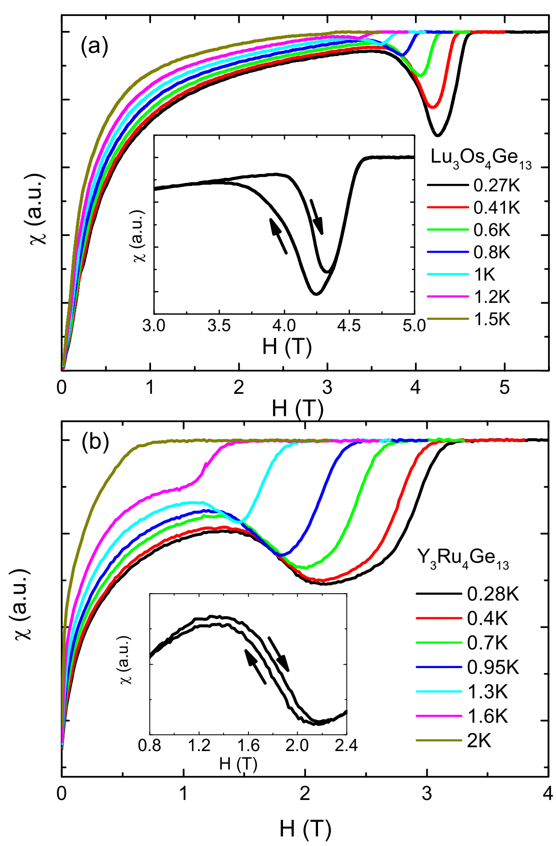

FIG. 5. (a) Isothermal ac susceptibility of $Lu_3Os_4Ge_{13}$ at different temperatures. The inset shows the magnified view of the hysteresis between up and down sweeps of the magnetic field at $T = 0.27$ K. (b) Isothermal ac susceptibility of $Y_3Ru_4Ge_{13}$ at different temperatures. The inset shows the magnified view of the hysteresis between up and down sweeps of the magnetic field at $T = 0.28$ K.

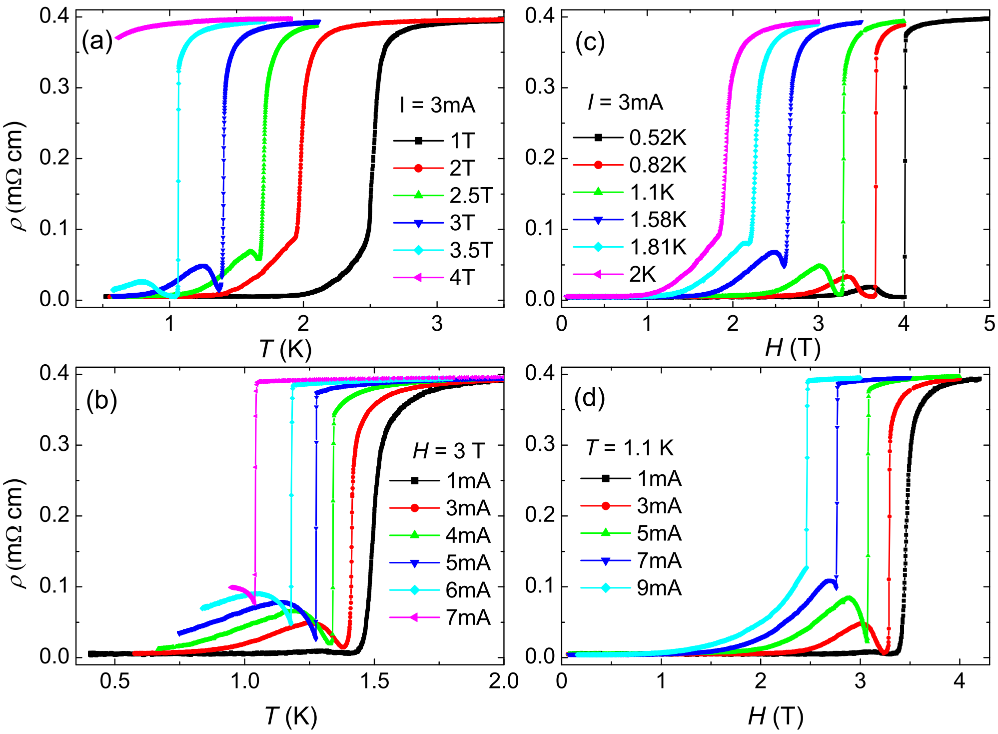

FIG. 6. Resistivity measurements of $Lu_3Os_4Ge_{13}$. The resistivity as a function of temperature is shown (a) for various applied fields for a current of $I = 3$ mA, and (b) for various currents when 3 T is applied. The field dependence of the resistivity is displayed (c) at various temperatures with $I = 3$ mA, and (d) for various currents at 1.1 K.

were then collected upon increasing and decreasing the field, and, for clarity, the main panels only show the down-sweeping curves. For $Lu_3Os_4Ge_{13}$ at 0.27 K, $\chi(H)$ increases with increasing field at low fields, reaching a peak at around 3.5 T before decreasing to a minimum at 4.25 T. This minimum lies below the upper critical field H_{c2}, above which $\chi(H)$ flattens. As displayed in the inset, the curves measured with increasing and decreasing field split in the region where $\chi(H)$ has a negative slope, whereas $\chi(H)$ is reversible at lower fields. With increasing temperature, the magnitude of the decrease above the peak reduces and at around 1.5 K, the anomaly is barely resolvable. The size of the hysteresis in the vicinity of the anomaly also decreases with increasing temperature. A similar anomaly is also seen in $Y_3Ru_4Ge_{13}$, where the local minimum is present at around 2.8 T at 0.28 K. Compared to $Lu_3Os_4Ge_{13}$, the magnitude of the dip above the peak is more shallow and, as displayed in the inset, the hysteresis is also reduced. The ac susceptibility measurements indicate the presence of the peak effect in both compounds, where in a certain field range near H_{c2}, there is an increase of the critical current J_c with increasing field instead of a decrease, which also accounts for the greater hysteresis between the up-sweeping and down-sweeping measurements.

Figure 6(a) shows the temperature dependence of the resistivity of $Lu_3Os_4Ge_{13}$ under various magnetic fields with a current of $I = 3$ mA. In applied magnetic fields of 1 and 2 T, after a sharp drop at the transition, there is a broad tail at lower temperatures where the resistivity is nonzero. At larger magnetic fields in the range of 2.5–3.5 T, a peak in the resistivity appears below T_c. When 3.5 T is applied, it can be clearly seen that upon cooling through the transition, zero resistivity is reached, but when the sample is cooled further, the resistivity becomes finite, indicating the presence of dissipative processes in the superconducting state, which disappear close to H_{c2} at high fields. At 4 T only a very weak downturn is observed despite the clear transition in the ac susceptibility for these fields, but this could also arise due to self-heating as a result of the fairly large current. The temperature dependence of the resistivity is shown for different currents in an applied field of 3 T in Fig. 6(b). For larger currents, the transition is seen at lower temperatures, which is again likely due to self-heating. At 1 mA, a significant finite resistivity is not observed below the transition, but at higher currents a peak is observed, with the maximum resistivity increasing with increasing current. This suggests that the finite resistivity arises in the superconducting state due to the current inducing a sufficiently large Lorentz force to cause the movement of vortices and therefore leading to dissipation. The unpinning of vortices within the superconducting state was also inferred from magnetization measurements at low fields [10]. The field dependence of the resistivity is shown for $I = 3$ mA at various temperatures in Fig. 6(c). Upon increasing the field at 0.52 K, the resistivity remains zero up to around 2.8 T, before it begins to increase, reaching a maximum at about 3.6 T. At higher fields the resistivity decreases, reaching zero again at around 3.9 T, and it remains zero until a sharp jump to the normal state at about 4 T. At higher temperatures, the peak moves to lower field and is clearly seen up to at least 1.58 K. At still higher temperatures, a finite resistivity is still found in the superconducting state, but without a clear peak. For different currents at a fixed temperature [Fig. 6(d)], the peak moves to a lower field with increasing current until it cannot be clearly resolved.

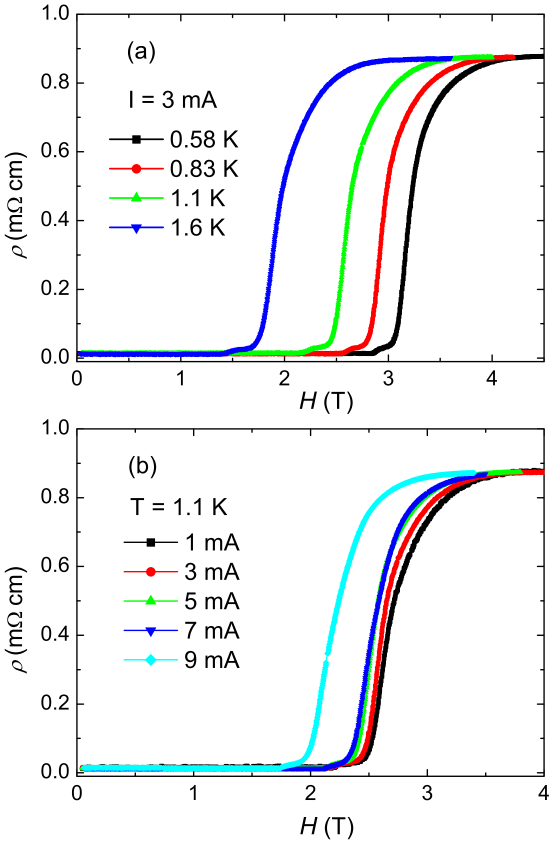

FIG. 7. Resistivity measurements of $Y_3Ru_4Ge_{13}$, (a) as a function of field at various temperatures with a current of $I = 3$ mA and (b) as a function of field at 1.1 K with various currents.

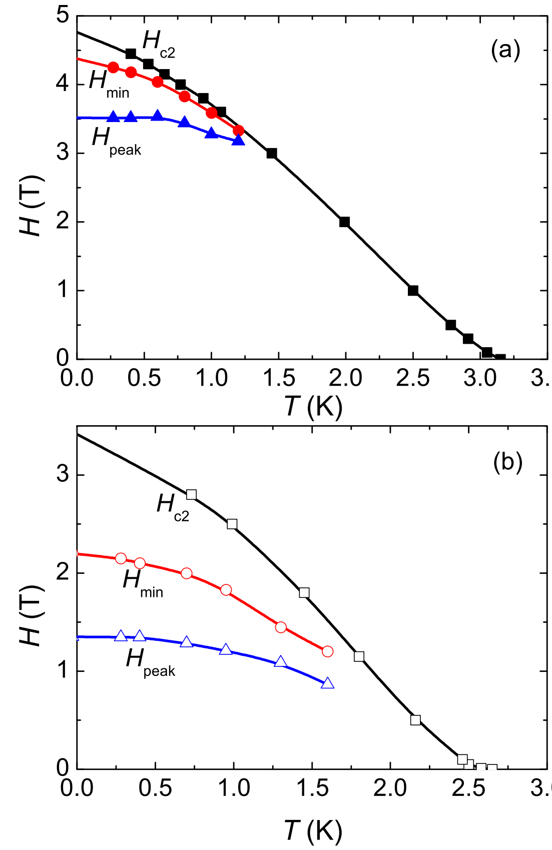

FIG. 8. Field-temperature phase diagram of (a) $Lu_3Os_4Ge_{13}$ and (b) $Y_3Ru_4Ge_{13}$. The black squares display the values of the upper critical field H_{c2} obtained from the temperature dependence of the ac susceptibility, while the red circles and blue triangles display the positions of the minima ($H_{\min}$) and maxima ($H_{\rm peak}$) in the field dependence of the ac susceptibility.

In contrast, for $Y_3Ru_4Ge_{13}$, a finite resistivity is not observed at low fields, and as displayed in Fig. 7, for all measured currents and temperatures, the resistivity only becomes nonzero just below the transition to the normal state at H_{c2}. Therefore, in the low-field region, the Lorentz force is not sufficiently strong to unpin vortices and lead to significant current dissipation, but just below H_{c2} the pinning is weak enough for vortices to move.

The field-temperature phase diagrams for both materials are displayed in Fig. 8, where H_{c2} is determined from the onset of the transition in the ac susceptibility, while $H_{\min}$ and $H_{\rm peak}$ correspond to the minima and maxima of the field-dependent ac susceptibility, respectively. Extrapolating to zero temperature gives respective values of $H_{c2}(0)$ of 4.8 and 3.4 T for $Lu_3Os_4Ge_{13}$ and $Y_3Ru_4Ge_{13}$. In addition, $H_{c2}(T)$ of both compounds show an upturn with decreasing temperature near T_c. This behavior has often been observed in multiband superconductors [32], and is therefore further evidence for two-gap superconductivity. The observation of the peak effect indicates that at low temperatures, there is a region of the phase diagram where J_c increases with increasing field, indicating a change from a more weakly pinned region at low fields to stronger pinning at high fields. In $Lu_3Os_4Ge_{13}$ the pinning at low fields is sufficiently weak that the resistivity becomes nonzero in the mixed state, but the stronger pinning at high fields leads to the peak features observed in Fig. 6, whereas in $Y_3Ru_4Ge_{13}$ the flux lines remain static in the region with weaker pinning at low fields. The stronger pinning in $Y_3Ru_4Ge_{13}$ compared to $Lu_3Os_4Ge_{13}$ is consistent with a larger normal state resistivity, indicating greater disorder. The occurrence of the peak effect has been explained as arising due to the rigidity of the flux line lattice disappearing with field more rapidly than the pinning force [33]. Peak effect behavior has been observed in various superconductors such as $CeRu_2$ [34,35], $2H$–$NbSe_2$ [36,37], and V_3Si [38]. It is also a common phenomenon in $R_3T_4Sn_{13}$ materials, having been observed in $Yb_3Rh_4Sn_{13}$ [39,40], $Ca_3Rh_4Sn_{13}$ [41], and $Ca_3Ir_4Sn_{13}$ [42], and this may correspond to a change from a well-ordered vortex lattice, to a disordered or partially ordered vortex glass phase [42–46].

IV. SUMMARY

In summary, we have performed measurements of the London penetration depth $\Delta\lambda(T)$ of $Lu_3Os_4Ge_{13}$ and $Y_3Ru_4Ge_{13}$ single crystals using a TDO-based technique down to 0.4 K. In both materials the behavior of $\Delta\lambda(T)$ at low temperatures clearly indicates nodeless superconductivity, while the analysis of $\Delta\lambda(T)$ and the superfluid density $\rho_s(T)$ gives evidence for the presence of multiple gaps. We also mapped the field-temperature phase diagram, and at low temperatures we find the peak effect in the ac susceptibility, which corresponds to an increase of J_c with field, as also reported in some of the isostructural stannides. Further work is required to understand the arrangement of vortices in the mixed state of these materials, and whether this behavior leads to the disordering of the vortex lattice at high fields, which require further measurements such as small angle neutron scattering.

ACKNOWLEDGMENTS

We thank F. Steglich, Q. H. Chen, and X. Lu for valuable discussions. This work was supported by the National Natural Science Foundation of China (Grants No. U1632275 and No. 11474251), National Key Research and Development Program of China (Grant No. 2016YFA0300202), and the Science Challenge Project of China.

[1] J. Remeika, G. Espinosa, A. Cooper, H. Barz, J. Rowell, D. McWhan, J. Vandenberg, D. Moncton, Z. Fisk, L. Woolf *et al.*, A new family of ternary intermetallic superconducting/magnetic stannides, Solid State Commun. **34**, 923 (1980).

[2] J. Hodeau, J. Chenavas, M. Marezio, and J. Remeika, The crystal structure of $SnYb_3Rh_4Sn_{12}$, a new ternary superconducting stannide, Solid State Commun. **36**, 839 (1980).

[3] R. Gumeniuk, L. Akselrud, K. O. Kvashnina, W. Schnelle, A. A. Tsirlin, C. Curfs, H. Rosner, M. Schöneich, U. Burkhardt, U. Schwarz *et al.*, $Ca_3Pt_{4+x}Ge_{13-y}$ and $Yb_3Pt_4Ge_{13}$: New derivatives of the $Pr_3Rh_4Sn_{13}$ structure type, Dalton Trans. **41**, 6299 (2012).

[4] R. Gumeniuk, M. Nicklas, L. Akselrud, W. Schnelle, U. Schwarz, A. A. Tsirlin, A. Leithe-Jasper, and Y. Grin, $Y_3Pt_4Ge_{13}$: A superconductor with a noncentrosymmetric crystal structure, Phys. Rev. B **87**, 224502 (2013).

[5] R. Gumeniuk, K. O. Kvashnina, W. Schnelle, A. Leithe-Jasper, and Y. Grin, Magnetic and transport properties of structural variants of Remeika phases: $Th_3Ir_4Ge_{13}$ and $U_3Ir_4Ge_{13}$, Phys. Rev. B **91**, 094110 (2015).

[6] H. Hayamizu, N. Kase, and J. Akimitsu, Superconducting properties of $Ca_3T_4Sn_{13}$ (T = Co, Rh, and Ir), J. Phys. Soc. Jpn. **80**, SA114 (2011).

[7] N. Kase, H. Hayamizu, and J. Akimitsu, Superconducting state in the ternary stannide superconductors $R_3T_4Sn_{13}$ (R = La, Sr; T = Rh, Ir) with a quasiskutterudite structure, Phys. Rev. B **83**, 184509 (2011).

[8] A. Ślebarski, M. Fijałkowski, M. M. Maśka, M. Mierzejewski, B. D. White, and M. B. Maple, Superconductivity of $La_3Co_4Sn_{13}$ and $La_3Rh_4Sn_{13}$: A comparative study, Phys. Rev. B **89**, 125111 (2014).

[9] K. Ghosh, S. Ramakrishnan, and G. Chandra, Resistivity and magnetic-susceptibility studies in the $R_3Ru_4Ge_{13}$ (R = Nd, Dy, Ho, Er, Yb, Lu, and Y) system, Phys. Rev. B **48**, 10435 (1993).

[10] O. Prakash, A. Thamizhavel, and S. Ramakrishnan, Multiband superconductivity in $Lu_3Os_4Ge_{13}$, Supercond. Sci. Technol. **28**, 115012 (2015).

[11] O. Prakash, A. Thamizhavel, A. Nigam, and S. Ramakrishnan, Superconductivity in a low carrier density system: A single crystal study of cubic $Y_3Ru_4Ge_{13}$, Physica C (Amsterdam) **492**, 90 (2013).

[12] A. M. Strydom, Superconductivity magnetism and atomic rattling phenomena in $R_3Rh_4Ge_{13}$ (R = Y, Yb, Lu), Acta Phys. Pol., A **126**, 318 (2014).

[13] B. K. Rai, I. W. H. Oswald, J. K. Wang, G. T. McCandless, J. Y. Chan, and E. Morosan, Superconductivity in single crystals of $Lu_3T_4Ge_{13-x}$ (T = Co, Rh, Os) and $Y_3T_4Ge_{13-x}$ (T = Ir, Rh, Os), Chem. Mater. **27**, 2488 (2015).

[14] Y. Mudryk, A. Grytsiv, P. Rogl, C. Dusek, A. Galatanu, E. Idl, H. Michor, E. Bauer, C. Godart, D. Kaczorowski *et al.*, Physical properties and superconductivity of skutterudite-related $Yb_3Co_{4.3}Sn_{12.7}$ and $Yb_3Co_4Ge_{13}$, J. Phys.: Condens. Matter **13**, 7391 (2001).

[15] H. Sato, T. Fukuhara, S. Iwakawa, Y. Aoki, I. Sakamoto, S. Takayanagi, and N. Wada, Magnetic and transport properties of $RE_3Ir_4Sn_{13}$, Physica B (Amsterdam) **186**, 630 (1993).

[16] C. Nagoshi, R. Yamamoto, K. Kuwahara, H. Sagayama, D. Kawana, M. Kohgi, H. Sugawara, Y. Aoki, H. Sato, T. Yokoo *et al.*, Magnetic and transport properties of $Gd_3Ir_4Sn_{13}$ with unique crystal structure, J. Phys. Soc. Jpn. **75**, 044710 (2006).

[17] O. Prakash, A. Thamizhavel, and S. Ramakrishnan, Ferromagnetic ordering of minority Ce^{3+} spins in a quasiskutterudite $Ce_3Os_4Ge_{13}$ single crystal, Phys. Rev. B **93**, 064427 (2016).

[18] M. F. Hundley, J. L. Sarrao, J. D. Thompson, R. Movshovich, M. Jaime, C. Petrovic, and Z. Fisk, Unusual Kondo behavior in the indium-rich heavy-fermion antiferromagnet $Ce_3Pt_4In_{13}$, Phys. Rev. B **65**, 024401 (2001).

[19] A. Strydom, N. Oeschler, and F. Steglich, $R_3Ir_4Ge_{13}$ (R = Yb, Lu): Thermal and magnetic properties, Physica B (Amsterdam) **403**, 746 (2008).

[20] B. K. Rai and E. Morosan, Intermediate valence in single crystals of $(Lu_{1-x}Yb_x)_3Rh_4Ge_{13}$ $(0 \leqslant x \leqslant 1)$, APL Mater. **3**, 041511 (2015).

[21] B. K. Rai, I. W. H. Oswald, J. Y. Chan, and E. Morosan, Intermediate valence to heavy fermion through a quantum phase transition in $Yb_3(Rh_{1-x}T_x)_4Ge_{13}$($T$ = Co,Ir) single crystals, Phys. Rev. B **93**, 035101 (2016).

[22] L. E. Klintberg, S. K. Goh, P. L. Alireza, P. J. Saines, D. A. Tompsett, P. W. Logg, J. Yang, B. Chen, K. Yoshimura, and F. M. Grosche, Pressure- and Composition-Induced Structural Quantum Phase Transition in the Cubic Superconductor $(Sr,Ca)_3Ir_4Sn_{13}$, Phys. Rev. Lett. **109**, 237008 (2012).

[23] S. K. Goh, D. A. Tompsett, P. J. Saines, H. C. Chang, T. Matsumoto, M. Imai, K. Yoshimura, and F. M. Grosche, Ambient Pressure Structural Quantum Critical Point in the Phase Diagram of $(Ca_xSr_{1-x})_3Rh_4Sn_{13}$, Phys. Rev. Lett. **114**, 097002 (2015).

[24] K. Wang and C. Petrovic, $Ca_3Ir_4Sn_{13}$: A weakly correlated nodeless superconductor, Phys. Rev. B **86**, 024522 (2012).

[25] S. Y. Zhou, H. Zhang, X. C. Hong, B. Y. Pan, X. Qiu, W. N. Dong, X. L. Li, and S. Y. Li, Nodeless superconductivity in $Ca_3Ir_4Sn_{13}$: Evidence from quasiparticle heat transport, Phys. Rev. B **86**, 064504 (2012).

[26] S. Gerber, J. L. Gavilano, M. Medarde, V. Pomjakushin, C. Baines, E. Pomjakushina, K. Conder, and M. Kenzelmann,

Microscopic studies of the normal and superconducting state of $Ca_3Ir_4Sn_{13}$, Phys. Rev. B **88**, 104505 (2013).
[27] W. C. Yu, Y. W. Cheung, P. J. Saines, M. Imai, T. Matsumoto, C. Michioka, K. Yoshimura, and S. K. Goh, Strong Coupling Superconductivity in the Vicinity of the Structural Quantum Critical Point in $(Ca_xSr_{1-x})_3Rh_4Sn_{13}$, Phys. Rev. Lett. **115**, 207003 (2015).
[28] P. K. Biswas, Z. Guguchia, R. Khasanov, M. Chinotti, L. Li, K. Wang, C. Petrovic, and E. Morenzoni, Strong enhancement of s-wave superconductivity near a quantum critical point of $Ca_3Ir_4Sn_{13}$, Phys. Rev. B **92**, 195122 (2015).
[29] B. Pavan and M. Fornari, Exploring potential thermoelectric materials: Electronic structure calculations of $Y_3Ru_4Ge_{13}$ and related compounds, Sci. Adv. Mater. **3**, 587 (2011).
[30] R. Prozorov, R. W. Giannetta, A. Carrington, and F. M. Araujo-Moreira, Meissner-London state in superconductors of rectangular cross section in a perpendicular magnetic field, Phys. Rev. B **62**, 115 (2000).
[31] A. Carrington and F. Manzano, Magnetic penetration depth of MgB_2, Physica C (Amsterdam) **385**, 205 (2003).
[32] M. Zehetmayer, A review of two-band superconductivity: Materials and effects on the thermodynamic and reversible mixed-state properties, Supercond. Sci. Technol. **26**, 043001 (2013).
[33] A. B. Pippard, A possible mechanism for the peak effect in type II superconductors, Philos. Mag. **19**, 217 (1969).
[34] A. D. Huxley, C. Paulson, O. Laborde, J. L. Tholence, D. Sanchez, A. Junod, and R. Calemczuk, Flux pinning, specific heat and magnetic properties of the Laves phase superconductor $CeRu_2$, J. Phys.: Condens. Matter **5**, 7709 (1993).
[35] N. Dilley, J. Herrmann, S. Han, M. Maple, S. Spagna, J. Diederichs, and R. Sager, Anomalous electrical resistivity in the superconducting state of $CeRu_2$, Physica C (Amsterdam) **265**, 150 (1996).
[36] S. Bhattacharya and M. J. Higgins, Peak effect and anomalous flow behavior of a flux-line lattice, Phys. Rev. B **49**, 10005 (1994).
[37] S. Ramakrishnan, K. Ghosh, A. Grover, G. I. Menon, T. C. Rao, G. Ravikumar, P. Mishra, V. Sahni, C. Tomy, G. Balakrishnan *et al.*, On the magnetic study of the peak effect in the anisotropic superconductor $2H$-$NbSe_2$ evidence for reentrant behavior, Physica C (Amsterdam) **256**, 119 (1996).
[38] M. Isino, T. Kobayashi, N. Toyota, T. Fukase, and Y. Muto, Magnetization and peak effect of several single crystals of V_3Si, Phys. Rev. B **38**, 4457 (1988).
[39] H. Sato, Y. Aoki, H. Sugawara, and T. Fukuhara, Peak effect in the superconducting mixed state of $Yb_3Rh_4Sn_{13}$ single crystals, J. Phys. Soc. Jpn. **64**, 3175 (1995).
[40] C. V. Tomy, G. Balakrishnan, and D. McK. Paul, Regions of enhanced pinning in the mixed state of the superconductor $Yb_3Rh_4Sn_{13}$, Physica C (Amsterdam) **280**, 1 (1997).
[41] C. V. Tomy, G. Balakrishnan, and D. McK. Paul, Observation of the peak effect in the superconductor $Ca_3Rh_4Sn_{13}$, Phys. Rev. B **56**, 8346 (1997).
[42] S. Kumar, R. P. Singh, A. Thamizhavel, C. Tomy, and A. Grover, Dual role of an ac driving force and the underlying two distinct order-disorder transitions in the vortex phase diagram of $Ca_3Ir_4Sn_{13}$, Physica C (Amsterdam) **506**, 69 (2014).
[43] S. Sarkar, D. Pal, S. S. Banerjee, S. Ramakrishnan, A. K. Grover, C. V. Tomy, G. Ravikumar, P. K. Mishra, V. C. Sahni, G. Balakrishnan *et al.*, Stepwise amorphization of the flux-line lattice in $Ca_3Rh_4Sn_{13}$: A peak-effect study, Phys. Rev. B **61**, 12394 (2000).
[44] S. Sarkar, D. Pal, P. L. Paulose, S. Ramakrishnan, A. K. Grover, C. V. Tomy, D. Dasgupta, B. K. Sarma, G. Balakrishnan, and D. McK. Paul, Multiple magnetization peaks in weakly pinned $Ca_3Rh_4Sn_{13}$ and $YBa_2Cu_3O_{7-\delta}$, Phys. Rev. B **64**, 144510 (2001).
[45] D. Mazzone, J. L. Gavilano, R. Sibille, M. Ramakrishnan, and M. Kenzelmann, Small-angle neutron scattering study of the mixed state of $Yb_3Rh_4Sn_{13}$, Phys. Rev. B **90**, 020507 (2014).
[46] D. G. Mazzone, J. L. Gavilano, R. Sibille, M. Ramakrishnan, C. D. Dewhurst, and M. Kenzelmann, Distinct vortex-glass phases in $Yb_3Rh_4Sn_{13}$ at high and low magnetic fields, J. Phys.: Condens. Matter **27**, 245701 (2015).